Slow Energy Transfer in Self-Doped β-Conformation Film of Steric Polydiarylfluorenes toward Stable Dual Deep-Blue Amplified Spontaneous Emission

M. Xu,[1] L. Sun,[2] S. Wang, [2] J. Lin,*[2] M. Yu,[1] X. Wang,[3] P. N. Stavrinou,[4] L. Xie,[1]
N. J. Cheetham,*[3] X. Ding,[2] D. D. C. Bradley,*[4,5] W. Huang*[1]

[1]National Key Laboratory for Organic Electronics and Information Displays & Institute of Advanced Materials (IAM),
Nanjing University of Posts & Telecommunications,
9 Wenyuan Road, Nanjing 210023, China.
E-mail: wei-huang@njtech.edu.cn

[2]Center for Supramolecular Optoelectronics (CSO), Key Laboratory of Flexible Electronics (KLOFE) & Institute of Advanced Materials (IAM),
Nanjing Tech University (NanjingTech),
30 South Puzhu Road, Nanjing 211816, China.
E-mail: iamjylin@njtech.edu.cn

[3]Department of Physics and Centre for Plastic Electronics,
The Blackett Laboratory, Imperial College London,
Prince Consort Road, London SW7 2AZ, UK.
E-mail: n.cheetham13@imperial.ac.uk

[4]Departments of Engineering Science & Physics,
Division of Mathematical, Physical & Life Sciences, University of Oxford,
9 Parks Road, Oxford OX1 3PD, UK.

[5]Physical Science and Engineering Division,
King Abdullah University of Science and Technology,
Thuwal 23955-6900, Saudi Arabia.
E-mail: donal.bradley@kaust.edu.sa

Keywords: Polydiarylfluorenes, β-Conformation, Time-resolved PL Spectroscopy, Energy Transfer, Dual wavelength amplified spontaneous emission

Abstract. Exciton behavior is crucial for improving the optoelectronic properties of light-emitting conjugated polymers. Herein, the photoexcitation dynamics of exciton migration and energy transfer in self-doped *β*-conformation film of the polydiarylfluorene, poly[4-(octyloxy)-9,9-diphenylfluoren-2,7-diyl]-co-[5-(octyloxy)-9,9-diphenylfluoren-2,7-diyl] (PODPF) are demonstrated. Compared to the first generation of the *β*-conformation polyfluorene, poly(9,9-dioctylfluorene) (PFO), energy transfer occurs in PODPF *β*-conformation films in a time period of ~150 ps, much longer than for PFO films (< 5 ps), associated with the effective intrachain energy transfer (few hundred picoseconds), rather than interchain Förster energy transfer (a few picoseconds). Similar to PFO, the PODPF *β*-conformation also displays well-resolved vibronic emission peaks at 20 K, attributed to the planar and rigid conformation. Interestingly, a residual 0-0 band emission of non-planar conformation chain segments (435 nm, 2.85 eV at 20 K) also further confirms the exciton migration paths from the disordered state to the *β*-conformation domains in PODPF films. The stable dual amplified spontaneous emission (ASE) behavior of the PODPF self-doped films observed at 461 nm (2.69 eV) and 483 nm (2.57 eV) at room temperature, originates from both the disordered and *β*-conformation domains.

1. Introduction: Intra-chain π-Electron delocalization of conjugated polymers is a fundamental factor to control a variety of processes spanning from charge transport to the photo-physics of neutral excited species or charged states.[1] In general, conjugated chains consist of many aromatic units with an σ-bond as a link, which enable their one-dimensional (1D) *p*-orbital overlap along the conjugated backbone.[2] The long-range structural chain conformation can precisely control exciton diffusion, charge transport and energy transfer.[1, 2a, 3] Compared to non-planar conformation chains, planar conformation chains have a longer effective conjugation length, a narrower optical-gap and more anisotropic

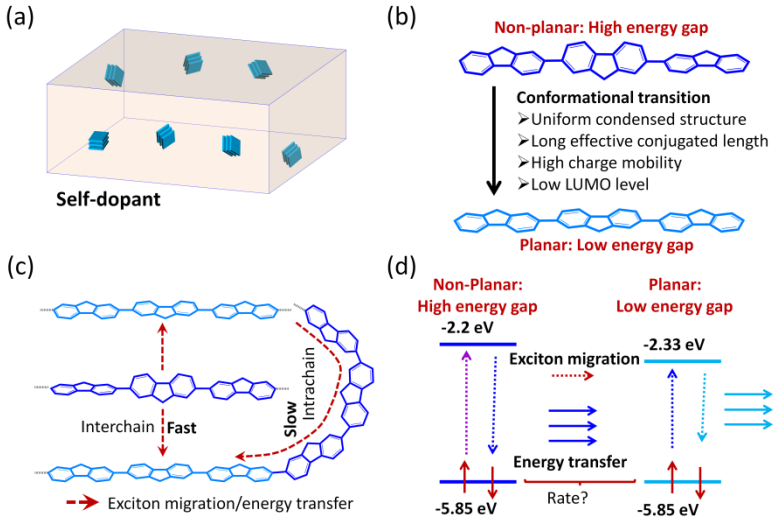

***Scheme* 1**. Self-dopant formation in conjugated polymer by controlling intrachain conformation. (a) Self-dopant formation in spin-coated films.[7] (b) Conformation transition of polyfluorene. Text describes the novel properties of planar conformation chain segments, compared to non-planar conformation segments.[4c] (c) Route of intra- and inter-chain exciton migration and energy transfer.[1a, 10, 11] Inter-chain energy transfer located within a Förster transfer radius is much faster than for intra-chain transfer (up to two orders of magnitude).[11] (d) Schematic showing the energy transfer and exciton migration from disordered matrix to planar conformation segments in this heterogeneous system.[4b, 10]

optoelectronic behaviour, which is desirable to meet the requirement of various optoelectronic devices.[1d, 4] However, as a consequence of the low rotational energy barrier along the conjugated backbone, the metastable planar conformation is preferentially stabilized by rigid environments.[5] In addition, it is highly challenging to obtain homogeneous and uniform films with a fully-planar chain conformation, but self-doped structures comprising ordered chain segments randomly distributed in a disordered matrix (*Scheme* 1a) are possible.[1e, 4b, 7] The ordered chains will act as guest energy sinks to trap excitons and energy from the matrix non-planar conformation chains (*Scheme* 1b).[1e, 7, 8] Multiple conformations coexist in thin films of all conjugated polymers but obtaining a red-shifted absorption and emission behaviour, effective charge transport, and long exciton diffusion length for high performance optoelectronic devices needs careful conformation control.[9] Diverse inter-chain electronic

couplings assisted by non-covalent interactions exist and it is of great interest to fully explore the intra- and inter-chain exciton migration and energy transfer in such complicated condensed structures.

Linear-type conjugated chains can be defined as a number of segments with a distribution of effective conjugation length and energy gap (*Scheme* 1c).[1a, 1d, 2b] Exciton diffusion and energy transfer occurs along backbone structures from the non-planar conformation segments (host segments) to the relatively planar ones with a lower energy gap (also called guest segments) (*Scheme* 1d).[10] Inter-chain packing also enables effective π-electron coupling, with exciton migration via: Förster transfer, tunneling and thermally assisted hopping, where the transfer process and rate are associated with the local microscopic geometry and the molecular conformation.[8b, 10, 12] Previous studies,[10, 12a] showed that energy transfer from the non-planar conformation chains to the *β*-conformation chains in poly(9,9-dioctylfluorene) (PFO) occurs at a picosecond timescale, < 5 ps. This is attributed to the close proximity of non-planar and planar conformation chains, and the large spectral overlap between the emission spectra of the non-planar conformation chains and the absorption spectra of the planar chains.[8b, 10] Therefore, even at an extremely low fraction (< 0.4%) of the *β*-conformation in the film, the characteristic optical and electronic behaviour of the *β*-conformation chain is observed, and this is associated with the synergistic effect of the strong inter-chain interaction and fast exciton migration.[7] In this regard, the exciton diffusion in PFO *β*-conformation films may not precisely reveal the real intra-chain exciton migration and energy transfer.[8b, 10, 11] To further systematically investigate this exciton migration and energy transfer, we synthesised a second generation *β*-conformation polydiarylfluorene, namely poly[4-(octyloxy)-9,9-diphenylfluoren-2,7-diyl]-co-[5-(octyloxy)-9,9-diphenylfluoren-2,7-diyl] (PODPF), as a new example within which to explore exciton diffusion (Figure 1a).[4c, 5a, 9a, 13] Compared to PFO, steric units at the 9-position

can effectively suppress inter-chain π-π interaction and inter-chain packing to partially isolate the chain in the condensed state and thereby improve the emission spectral stability. According to previous work,[4b] the critical fraction to induce pure β-conformation emission for PFO was calculated to be $\leq 0.4\%$. As expected, the characteristic emission of the β-conformation chain for PODPF could only be observed at a critical fraction >10%, 25-fold higher than that of PFO films (Figure 1b). This result was consistent with previous work.[4c] In addition, energy transfer occurred from the non-planar conformation chains to the β-conformation chains in a time period of >150 ps, much longer than that of PFO. Fast energy transfer for pristine PFO β-conformation films leads to stable dual wavelength amplified spontaneous emission (ASE) not being obtained simultaneously from both the glassy and β-conformation chain segments. However, partial photoxidative degradation, that reduces the energy transfer rate from glassy PFO chain segments to β-conformation segments, does then allow ASE from both glassy and β-conformation chain segments.[9d] Consistent with this observation, the longer transfer time meant that it was possible to obtain stable dual ASE peaks at 461 nm (2.69 eV) and 483 nm (2.57 eV) for PODPF films. These results help to confirm the slower rate of energy transfer between the disordered and β-conformation chain segments in PODPF films as compared to PFO.

2. Results and Discussion

As discussed above, non-planar and planar conformations can coexist within fluorene-based conjugated polymer films.[1e, 7, 9d, e, 10] The ordered chain segments are randomly dispersed within a disordered matrix, following generation by various post-deposition treatment processes, such as low temperature thermal cycling, solvent additives, and solvent exposure in vapour or liquid form (*Scheme* 1a).[1e, 5a, b, 7, 9b, d, e, 10, 13]

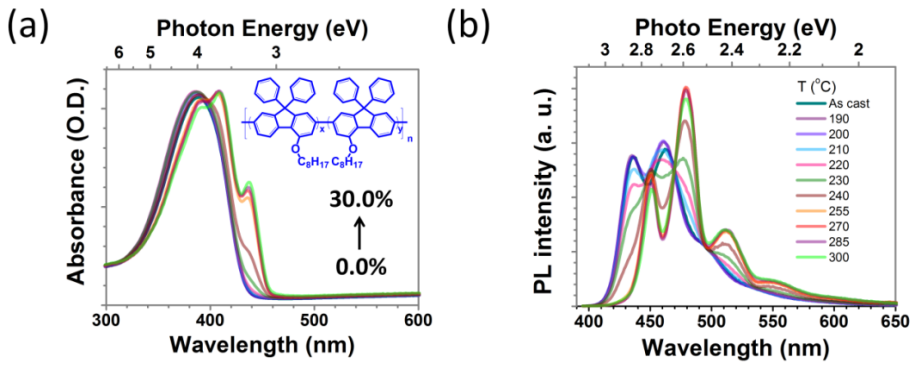

Figure 1. Optical properties of PODPF pristine and annealed films. (a) Absorbance and (b) PL spectra of PODPF films after thermal treatment at various annealing temperatures up to 300°C. Films were annealed at elevated temperatures in air for 3 min and measured at room temperature after cooling.

A significantly different approach to that for PFO-type systems, namely elevated temperature thermal treatment is a specific experimental method to induce chain planarization of PODPF. Such annealing for many PFO-type systems leads to crystallization.[7] Here, high *β*-conformation fractions >10% are possible, as required to ensure complete energy transfer from non-planar conformation chains to *β*-conformation chains, and thus obtain the characteristic emission spectra of the latter. Desirably, the fraction of PODPF *β*-conformational chains in amorphous matrix can be tuned by controlling the thermal annealing temperature.[5a, 9c] Figure 1a, b and Figures S1, S2 and S3 in the Supporting Information display the absorbance and photoluminescence (PL) spectra of PODPF pristine and variously annealed films (≈ 100 nm). As the annealing temperature is increased to 210 °C, the appearance of the characteristic extra absorbance peak at 444 nm and red-shifted PL spectra confirmed the formation of *β*-conformation PODPF chains in the annealed films. Films annealed at temperatures higher than 210 °C, showed a steady increase in the extra absorption band at 444 nm and associated changes in the PL emission spectral profile (Figure 1 and Figure S4 in the Supporting Information); this aligns with a thermal transition in differential scanning calorimetry curves at 212 °C in previous work.[5a] The critical temperature for PODPF *β*-conformation formation was estimated to be

210 °C (see tangent line in Figure S4 in Supporting Information). For higher temperatures, the *β*-conformation fraction rose sharply with increasing annealing temperature before then saturating at ≥ 255 °C. All of the absorption spectra presented broad peaks at ≈ 390 nm (3.18 eV) with the characteristic *β*-conformation peak at 444 nm (2.79 eV).[5a, 9a, 13] The former was attributed to the broadened $S_0 \rightarrow S_1$ transitions in the glassy PODPF matrix. In addition, a shoulder absorption peak at 410 nm (3.02 eV) was also clearly observed, a vibronic replica (0-1) of the 444 nm (0-0) *β*-conformation transition. The characteristic *β*-conformation absorption peaks are also clear in reflection corrected absorption spectra (Figure S1, Supporting Information). Additionally, as a result of longer effective conjugation length, the PL emission from the *β*-conformation chains was characterized by vibronic peaks at 450, 480, 512 and 550 nm (2.76, 2.58, 2.42 and 2.25 eV, respectively) while the emission peaks of non-planar conformation chains were seen at 436, 463 and 496 nm (2.84 eV, 2.68 eV and 2.50 eV, respectively). In both cases the peaks were attributed to vibronic transitions 0-0, 0-1 and 0-2 with, in the case of the *β*-conformation, an additional 0-3 peak, as seen in previous reports for PODPF.[4c, 5a, 9a, 13] Red-shifted and narrower linewidth PL peaks are consistent with the *β*-chains adopting a more highly ordered, rigid planar geometry, leading to lower inhomogeneous broadening, and a narrower energy gap than for non-planar conformation chains. [1e, 4c, 5a, 7] Figure S4 in the Supporting Information displays the fraction of *β*-conformation chains in the annealed film, and the fraction of emission from the *β*-conformation chains across several PODPF films (100 nm) as a function of annealing temperature. The exponential functions are fitted to explore the rate of energy transfer from disordered to *β*-conformation chains prior to emission for PFO and PODPF. Similar to PFO, the *β*-conformation PL fraction for PODPF was non-linear with *β*-conformation absorption fraction; it exhibited a shallower rise and didn't saturate until ≈ 97 %. This again confirms a much lower rate of energy transfer from the disordered chains to the *β*-conformation chains. The *β*-conformation fraction-dependent PL

spectra are also shown in Figure 1. The emission from the *β*-conformation chains increased, as expected, with the fraction of *β*-conformation chain absorption. Unlike PFO, however, the *β*-conformation emission of PODPF was only found at high *β*-conformation fractions. As above, the corresponding critical fraction of *β*-conformation for PODPF was estimated to be ≥ 10%, much higher than that for PFO (< 0.4%.).[4b] Additionally, we further explored this behaviour directly through time-resolved PL measurements on films containing varying fractions of *β*-conformation chains (Figure 2 and Figure S5 Supporting Information). According to our previous works,[4c, 9c] the *β*-conformation domains of PFO are larger in size than for PODPF.

Beyond inter-chain packing mediated transfer, intra-chain exciton migration and energy transfer should also be present for both PFO and PODPF. Inter-chain transfer is understood to generally be faster than intra-chain (Scheme 1) [9-10] but the steric unit at the 9-position for PODPF should be able to suppress this "fast"-type exciton migration and hence significantly reduce the transfer rate from non-planar conformation segments to planar ones.[5a, 12] In order to further check this hypothesis, we recorded time-resolved PL spectra for the disordered and *β*-conformation films (obtained at various delay times ranging from 0 to 600 ps with 50 and 100 ps time windows; Figure 2 and Figures S5, S6 and S7 in Supporting Information). No significant emission was observed from non-planar chains in such PL spectra (data not shown) for PFO *β*-conformation films even with a low fraction ≈ 1%, confirming that all the photoexcited excitons migrate rapidly to *β*-conformation segments. This fast energy transfer may be plausibly explained by the strong inter-chain exciton transfer for transfer distances within the Förster transfer radius ~8 nm. Similar to PFO disordered films,[8b, 10] the PODPF pristine films showed emission spectra that varied little from 0 ps to 600 ps (Figure S7 in Supporting Information). PODPF *β*-conformation films, in contrast, show significant changes in time (Figure 2 and Figures S5 and S6 in Supporting Information) and by separating the

kinetics for the different spectral contributions, we can estimate the *β*-conformation PL emission fraction as a function of delay time. The *β*-conformation PL fraction is constant at ≈ 30% up to ~ 150 ps, close to where the peak in the integrated signal is reached. The fraction then increases for times out to 600 ps, as the overall (integrated) signal falls. A constant fraction would be consistent with an absence of energy transfer during the pump pulse (Δt_{FWHM} = ~ 60 ps), as both disordered and *β*-conformation chains will be excited through absorption at 379 nm (3.27 eV) and the system is in a quasi-steady-state 'equilibrium'. The subsequent rising *β*-conformation PL fraction shows that energy transfer is taking place over these extended times. The flexible alkyl chains at the fluorene C9-position for PFO versus the rigid phenyl rings for PODPF allow PFO to show stronger interchain interactions with a smaller separation distance (~ 0.4 nm) and hence to support "faster" inter-chain transfer. Inter-chain exciton migration is, however, relatively suppressed for PODPF compared to "slow" intra-chain transfer.

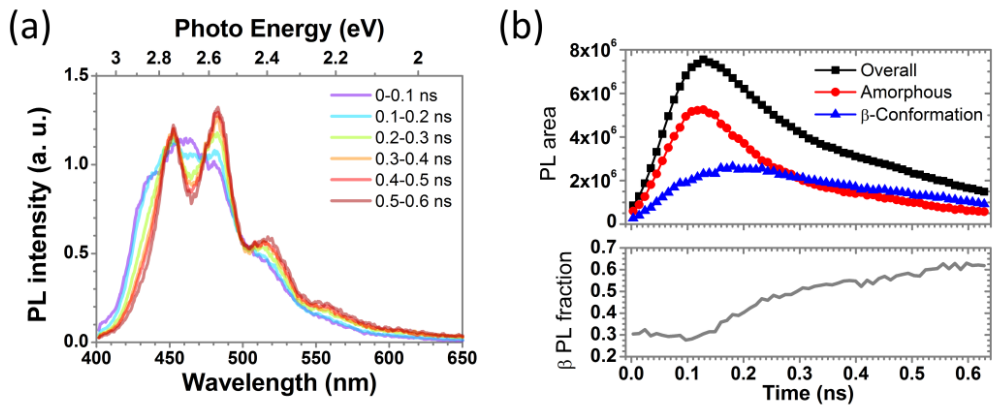

Figure 2. (a) Time-resolved PL spectra of PODPF annealed film obtained at different delay times in the range from 0 to 600 ps. (b) Integrated PL area as a function of time for PODPF annealed film with 20 % *β*-conformation fraction, showing energy transfer from disordered to *β*-conformation chains. The separated non-planar and *β*-conformation contributions are obtained by spectral subtraction methods. The bottom curve shows the variation in the fractional *β*-conformation contribution to the PL spectra as a function of time.

Temperature affects molecular vibration and conformation and we have, therefore, also measured temperature-dependent PL spectra to further probe exciton migration and energy transfer in PODPF films.[1g, h, 4e, 7, 10] Figure 3a shows the red-shifting and narrowing of the vibronic emission lines for a 20% *β*-conformation PODPF film with decreasing temperature, also revealing fine structure due to the presence of different modes coupled to the electronic transition. This appears as a splitting of the 0 → n ≥ 1 vibronic bands, with up to the 0-4 vibronic band clearly resolved on the log scale. The linewidth of the 0-0 emission peak in the *β*-conformation films reduced at low temperature, from 6.2 nm (≈ 56 meV) at room temperature (RT) to 5 nm (≈ 25 meV) at 20 K. This is a result of exciton migration to the lowest energy-gap regions in a hierarchical energy structure with emission occurring predominantly from the deepest levels, also yielding the observed red-shift. In this regard, the hierarchical uniform artificial superstructure can provide an effective electronic landscape to promote exciton diffusion.[14] The reduction of the PL spectrum full-width at half-maximum (FWHM) further indicates that the planarity and long effective conjugation length of *β*-conformation chains increases as the temperature is reduced. Compared to room temperature (290K), the 20K 0-0 emission peak of PODPF *β*-conformation films is red-shifted by ≈ 4.0 nm closer to that of the fully planar MeLPPP. Figure 3b shows that the well-resolved vibronic progression at low temperature closely matches between *β*-conformation emission of PODPF and PFO, with the PODPF emission, however, red-shifted by ≈ 85 meV relative PFO. In contrast, the absorption peak of the *β*-conformation of PODPF was only red shifted by ≈ 20-30 meV relative to that of PFO at room temperature. Both the splitting between peaks and the relative intensities were closely matched. This suggested that vibrational modes of very similar energies and likely physical composition (e.g. stretching and bending) were strongly coupled to the radiative $S_1 \rightarrow S_0$ electronic transitions.

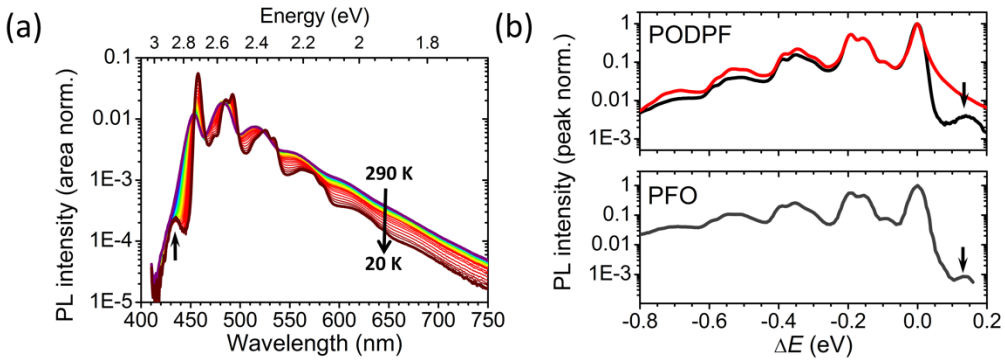

Figure 3. Low temperature PL spectra of the PODPF β-conformation self-doped fil. (a) Temperature-dependent area normalised PL spectra of PODPF annealed film (100 nm) with a β-conformation fraction of 20%. PL spectra were obtained for excitation at 405 nm and the temperature was varied from 290 K to 20 K. (b) Peak normalised experimental (black line) and theoretical (red line) PL spectra for PODPF (top panel) and experimental PL for PFO (bottom panel), with an energy x-axis showing the offset from the 0-0 vibronic peak at low temperature (20 K for PODPF and 12 K for PFO), exciting at 405 nm and 355 nm respectively.

In Figure 3b, we also plotted a theoretical PODPF emission spectrum calculated from its Raman mode energies and relative intensities as obtained from experimental ground state non-resonant Raman spectra. The methodology of the calculation is detailed in previous works.[15] The Raman intensities are allowed to vary in the calculation to fit the 0-0 and 0-1 vibronic bands of the experimental spectra between ΔE = -0.25 and 0.03 eV. For both materials, the experimental PL data were well reproduced well using similar experimental Raman modes at 1600, 1350 cm^{-1} for PODPF and 1601, 1352 cm^{-1} for PFO. As discussed above, the characteristic emission of the β-conformation for PODPF can only be obtained with a fraction of >10%. What is more, as displayed in Figure 3b, it is easy to observe that weak emission occurs with a peak at 2.85 eV with intensities ≈ 0.004 and 0.00083 for PODPF and PFO respectively. This is expected to originate from the residual 0-0 vibronic band emission of non-planar conformation chains. The emission intensity is 250 times (Intensity ratio: 1/0.004 = 250) weaker for PODPF self-doped films than disordered films. The corresponding 0-0 emission peak from non-coplanar conformation chains in β-conformation PFO films at 20K is 1200

times lower (Intensity ratio 1/0.00083 = 1200). This confirms the weaker rate of exciton migration in PODPF self-doped films than in PFO.

In the last several years, many investigations have explored the effect of β-conformation formation on the photo-physical processes in PFO. Compared to the disordered films, the PFO β-conformation self-doped films exhibit deep-blue emission spectral stability, lower lasing threshold and higher device performance.[4b, c, e, 5a, 9b, d] As discussed above, the β-conformation microstructure can trap excitons from the disordered matrix. In addition, the fast energy transfer enables the self-doped film to easily obtain characteristic β-conformation emission, even at a < 0.4% fraction for PFO. Therefore, it is difficult to obtain a dual stable ASE behaviour from the non-planar and planar conformation chains in a single self-doped film.[4e, 9d] In fact, the ASE behaviours of the PFO β-conformation self-doped film show a relatively dramatic dependence on pump beam energy. An ASE peak from β-conformation chains is observed at low pump excitation but ASE from the glassy non-planar conformation arises on increasing pump excitation.[4e, 9d] This has been attributed to a reduction in the fast energy transfer rate following pump-induced chemical/structural changes.

Interestingly, as observed above, the mixed PL emission behaviour of disordered and β-conformation PODPF chains was readily obtained for self-doped films. The corresponding ASE spectra under various pump energies are shown in Figure 4a. Both disordered and β-conformation ASE are simultaneously observed, with peaks at 461 nm (2.69 eV) and 483 nm (2.57 eV), respectively. Their intensity ratio changed little as the excitation energy increased from 0.46 to 2.89 μJ/pulse (Figure 4a inset) and the corresponding ASE thresholds are very similar, ≈ 0.68 and ≈ 0.70 μJ/pulse (Figure S8 in Supporting Information).

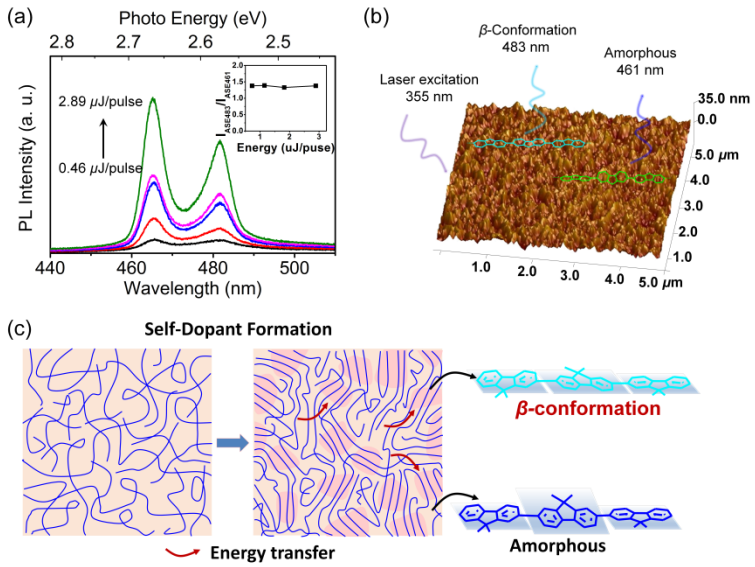

Figure 4. Dual ASE behaviour of PODPF *β*-conformation self-doped films obtained via thermal annealing at 230 °C. (a) ASE spectra of PODPF self-doped film with increasing excitation laser energy. Inset shows the intensity ratio of the ASE peaks at 483 nm and 461 nm upon increasing laser excitation pulse energy. (b) Atomic force microscope image of PODPF self-doped film. (c) Schematic showing the ASE behaviour of the multiple conformations in self-doped heterogeneous thin films.

3. Conclusion

We have reported a detailed investigation of the energy transfer processes in the second generation *β*-conformation polydiarylfluorene PODPF via room-temperature absorption, room- and low-temperature PL, time-resolved PL and ASE measurements (see Supporting Information for experimental details). As a result of increased steric interactions between chain segments, exciton migration in PODPF *β*-conformation films is relatively slow, with intra-chain energy transfer then key. The characteristic transfer time from disordered to *β*-conformation chain segments of ≈ 150 ps is much longer than the < 5 ps transfer time reported for PFO. Time-resolved PL spectroscopy for PODPF consequently reveals the clear signatures of spectral diffusion with red-shifted PL characteristic of the *β*-conformation growing in strength relative to the disordered non-planar conformation PL. In addition, as for the PFO *β*-conformation PL, very well-resolved vibronic peaks are also observed for PODPF *β*-

conformation films, and as for PFO are attributed to a rigid extended chain structure. Finally, stable dual deep-blue ASE emission is observed from the PODPF *β*-conformation self-doped films, a further consequence of slow exciton migration between the two exciton populations.

Acknowledgements

Man Xu and Lili Sun contributed equally to this work. It was supported by the National Natural Science Foundation of China (22075136, 61874053), National Key Research and Development Program of China (2020YFA0709900), Natural Science Funds of the Education Committee of Jiangsu Province (18KJA430009), Natural Science Foundation of Jiangsu Province (BK20200700), "High-Level Talents in Six Industries" of Jiangsu Province (XYDXX-019), Research Innovation in University of Jiangsu Province (KYCX21_0771), the open research fund from State Key Laboratory of Supramolecular Structure and Materials (sklssm202108) and Anhui Province Key Laboratory of Environment-friendly Polymer Materials. N.J.C., D.D.C.B. and P.N.S. thank the UK Engineering and Physical Sciences Research Council Doctoral Training Programme at the Imperial College London Centre for Plastic Electronics for providing PhD studentship support for Nathan Cheetham. D.D.C.B also thanks the Jiangsu Industrial Technology Research Institute (JITRI) IMPACT programme at the University of Oxford and the King Abdullah University of Science and Technology for additional support.

References

[1] a) A. J. Heeger, *Chem. Soc. Rev.* **2010**, *39*, 2354-2371; b) X. H. Jin, M. B. Price, J. R. Finnegan, C. E. Boott, J. M. Richter, A. Rao, S. M. Menke, R. H. Friend, G. R. Whittell, I. Manners, *Science* **2018**, *360*, 897-900; c) J. Lin, B. Liu, M. Yu, X. Wang, Z. Lin, X. Zhang, C. Sun, J. Cabanillas-Gonzalez, L. Xie, F. Liu, *Adv. Mater.* **2019**, *31*, 1804811.; d) W. Chunwaschirasiri, B. Tanto, D. L. Huber, M. J. Winokur, *Phys. Rev. Lett.* **2005**, *94*, 107402; e) N. J. Cheetham, M. Ortiz, A. Perevedentsev, L.-I. Dion-Bertrand, G. M.

Greetham, I. V. Sazanovich, M. Towrie, A. W. Parker, J. Nelson, C. Silva, D. D. C. Bradley, S. C. Hayes, P. N. Stavrinou, *Chem. Mater.* **2019**, *31*, 6787-6797. f) Y. Zhao, L. Liu, F. Zhang, C.-a. Di, D. Zhu, *SmartMat*, 2021, DOI: 10.1002/smm2.1034; g) A.J. Cadby, P.A. Lane, H. Mellor, S.J. Martin, M. Grell, C. Giebeler, D.D.C. Bradley, M. Wohlgenannt, C. An and Z.V. Vardeny, *Phys. Rev. B* **2000**, *62*, 15604-15609.; h) M. Ariu, D.G. Lidzey, M. Sims, A.J. Cadby, P.A. Lane and D.D.C. Bradley *J. Phys. Condens. Matter* **2002**, *14*, 9975-9986.

[2] a) K. Bong-Gi, J. Eun Jeong, C. Jong Won, S. Sungbaek, K. Bonwon, K. Jinsang, *Nature Mater.* **2013**, *12*, 659-664; b) L. H. Xie, C. R. Yin, W. Y. Lai, Q. L. Fan, W. Huang, *Prog. Polym. Sci.* **2012**, *37*, 1192-1264. c) Y. Wang, J. Yang, Y. Gong, M. Fang, Z. Li, B. Z. Tang, *SmartMat* **2020**, *1*, e1006. d) Y. Yao, Y. Chen, H. Wang, P. Samorì, *SmartMat* **2020**, *1*, e1009.

[3] A. T. Haedler, K. Kreger, A. Issac, B. Wittmann, M. Kivala, N. Hammer, J. Köhler, H.-W. Schmidt, R. Hildner, *Nature* **2015**, *523*, 196-199.

[4] a) P. Prins, F. C. Grozema, B. S. Nehls, T. Farrell, U. Scherf, L. D. A. Siebbeles, *Phys. Rev. B* **2006**, *74*, 113203; b) H. H. Lu, C. Y. Liu, C. H. Chang, S. A. Chen, *Adv. Mater.* **2010**, *19*, 2574-2579; c) M. N. Yu, H. Soleimaninejad, J. Y. Lin, Z. Y. Zuo, B. Liu, Y. F. Bo, L. B. Bai, Y. M. Han, T. A. Smith, M. Xu, *J. Phys. Chem. Lett.* **2018**, *9*, acs.jpclett.7b03148; d) H. Ling, J. Lin, M. Yi, B. Liu, W. Li, Z. Lin, L. Xie, Y. Bao, F. Guo, W. Huang, *Acs Appl. Mater. & Interfaces* **2016**, *8*, 18969; e) C. Rothe, F. Galbrecht, U. Scherf, A. P. Monkmam, *Adv. Mater.* **2006**, *18*, 2137-2140.

[5] a) B. Liu, J. Lin, F. Liu, M. Yu, X. Zhang, R. Xia, T. Yang, Y. Fang, L. Xie, W. Huang, *Acs Appl Mater Interfaces* **2016**, *8*, 21648-21655; b) K. Matti, A. P. Monkman, *Adv. Mater.* **2013**, *25*, 1090-1108; c) M. Arif, C. Volz, S. Guha, *Phys. Rev. Lett.* **2006**, *96*, 025503.

[6] a) N. J. Cheetham, M. Ortiz, A. Perevedentsev, L.-I. Dion-Bertrand, G. M. Greetham, I. V. Sazanovich, M. Towrie, A. W. Parker, J. Nelson, C. Silva, D. D. C. Bradley, S. C. Hayes, P. N. Stavrinou, *Chem. Mater.* **2019,** *31*, 6787-6797.; b) N. Rodrigo, R. Jonathan, V. Koen, F. P. V. Koch, S. Natalie, S. Paul, M. F. Toney, S. Alberto, *Nature Mater.* **2013**, *12*, 1037-1043.

[7] a) A. Hayer, A. L. T. Khan, R. H. Friend, A. Köhler, *Phys. Rev. B* **2005**, *71*, 241302; b) A. L. T. Khan, P. Sreearunothai, L. M. Herz, M. J. Banach, A. Köhler, *Phys. Rev. B* **2004**, *69*, 85201; c) F. L. Roux, D. D. C. Bradley, *Phys. Rev. B* **2018**, *98*, 195306.

[8] a) L. B. Bai, B. Liu, Y. M. Han, M. N. Yu, J. Wang, X. W. Zhang, C. J. Ou, J. Y. Lin, W. S. Zhu, L. Xie, *Acs Appl Mater Interfaces* **2017**, *9*, acsami.7b08980; b) X. Zhang, Q. Hu, J. Lin, Z. Lei, X. Guo, L. Xie, W. Lai, W. Huang, *Applied Physics Letters* **2013**, *103*, 153301; c) M. N. Yu, B. Liu, J. Y. Lin, L. Tao, L. Dan, L. Feng, W. S. Zhu, *Chinese Journal of Polymer Science* **2016**, *34*, 1311-1318; d) G. Ryu, R. Xia, D. D. C. Bradley, *Journal of Physics Condensed Matter* **2007**, *19*, 225-236; e) A. Perevedentsev, Y. Sonnefraud, C. R. Belton, S. Sharma, A. E. Cass, S. A. Maier, J. S. Kim, P. N. Stavrinou, D. D. C. Bradley, *Nature Communications* **2015**, *6*, 5977; f) S. M. Menke, R. J. Holmes, *Energy & Environmental Science* **2014**, *7*, 499-512.

[9] M. Ariu, M. Sims, M. D. Rahn, J. Hill, A. M. Fox, D. G. Lidzey, M. Oda, J. Cabanillasgonzalez, D. D. C. Bradley, *Phys. Rev. B,* **2003**, *67*, 195333.

[10] T.-Q. Nguyen, J. Wu, V. Doan, B. J. Schwartz, S. H. Tolbert, *Science* **2000**, *288*, 652-656.

[11] a) A. R. Buckley, M. D. Rahn, J. Hill, J. Cabanillas-Gonzalez, A. M. Fox, D. D. C. Bradley, *Chemical Physics Letters* **2001**, *339*, 331-336; b) E. J. W. List, C. Creely, G. Leising, N. Schulte, A. D. Schlüter, U. Scherf, K. Müllen, W. Graupner, *Chemical Physics Letters* **2000**, *325*, 132-138.

[12] J.-Y. Lin, W.-S. Zhu, F. Liu, L.-H. Xie, L. Zhang, R. Xia, G.-C. Xing, W. Huang, *Macromolecules* **2014**, *47*, 1001-1007.

[13] C. Ou, N. J. Cheetham, J. Weng, M. Yu, J. Lin, X. Wang, C. Sun, J. Cabanillas-Gonzalez, L. Xie, L. Bai, Y. Han, D. D. C. Bradley, W. Huang, *iScience* **2019**, *16*, 399-409.

[14] a) C. C. Wu, E. Ehrenfreund, J. J. Gutierrez, J. P. Ferraris, Z. V. Vardeny, *Physical Review B* **2005**, *71*, 081201; b) L. Tutt, D. Tannor, J. Schindler, E. J. Heller, J. I. Zink, *The Journal of Physical Chemistry* **1983**, *87*, 3017-3019.

Table of Contents Entry:

Energy transfer in *β*-conformation PODPF films occurs in a time ~150 ps, longer than in corresponding PFO films (< 5 ps), associated with intra-chain rather than inter-chain energy transfer. Stable dual wavelength ASE is observed as a consequence at 465 nm and 481 nm for self-doped films, derived from the individual disordered and *β*-conformation chain segments, respectively.

Man Xu, Lili Sun, Shengjie Wang, Jinyi Lin,* Mengna Yu, Xuhua Wang, Paul N. Stavrinou, Linghai Xie, Nathan J. Cheetham,* Xuehua Ding, Donal D. C. Bradley* and Wei Huang*

Slow Energy Transfer in Self-Doped *β*-Conformation Film of Steric Polydiarylfluorenes toward Stable Dual Deep-Blue Amplified Spontaneous Emission

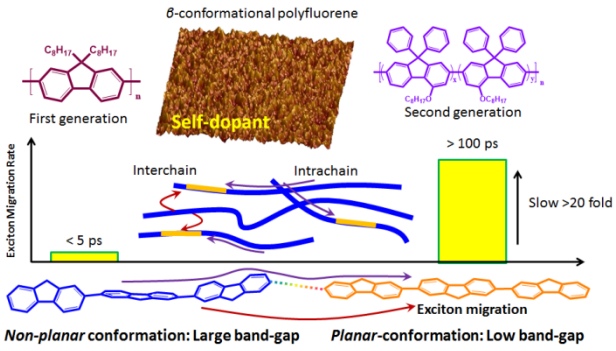

Supporting Information

Slow Energy Transfer in Self-Doped β-Conformation Film of Steric Polydiarylfluorenes toward Stable Dual Deep-Blue Amplified Spontaneous Emission

M. Xu,[1] L. Sun,[2] S. Wang,[2] J. Lin,*[2] M. Yu,[1] X. Wang,[3] P. N. Stavrinou,[4] L. Xie,[1]
N. J. Cheetham,*[3] X. Ding,[2] D. D. C. Bradley,*[4,5] W. Huang*[1]

[1]National Key Laboratory for Organic Electronics and Information Displays & Institute of Advanced Materials (IAM),
Nanjing University of Posts & Telecommunications,
9 Wenyuan Road, Nanjing 210023, China.
E-mail: wei-huang@njtech.edu.cn

[2]Center for Supramolecular Optoelectronics (CSO), Key Laboratory of Flexible Electronics (KLOFE) & Institute of Advanced Materials (IAM),
Nanjing Tech University (NanjingTech),
30 South Puzhu Road, Nanjing 211816, China.
E-mail: iamjylin@njtech.edu.cn

[3]Department of Physics and Centre for Plastic Electronics,
The Blackett Laboratory, Imperial College London,
Prince Consort Road, London SW7 2AZ, UK.
E-mail: n.cheetham13@imperial.ac.uk

[4]Departments of Engineering Science & Physics,
Division of Mathematical, Physical & Life Sciences, University of Oxford,
9 Parks Road, Oxford OX1 3PD, UK.

[5]Physical Science and Engineering Division,
King Abdullah University of Science and Technology,
Thuwal 23955-6900, Saudi Arabia.
E-mail: donal.bradley@kaust.edu.sa

Keywords: Polydiarylfluorenes, β-Conformation, Time-resolved PL Spectroscopy, Energy Transfer, Dual wavelength amplified spontaneous emission

Supplementary Materials

- **Figure S1**. (Left) Absorbance spectra for a 100 nm PODPF thin film before and after annealing sequentially for 3 minutes at increasing temperatures. The lower panel shows the change in absorbance spectra after annealing compared to the as cast film. (Right) The corresponding peak normalised photoluminescence (PL) spectra for the sequentially annealed PODPF film.
- **Figure S2.** Reflection corrected absorption spectra for 100 nm PODPF thin films after step-wise annealing in 15 °C steps from 210 °C to the temperature stated in the figure legend.
- **Figure S3**. Example absorbance and PL spectra separated into disordered (A) and *β*-conformation components, using Gaussian peak fitting and normalisation and subtraction methods. The annealing temperature for the samples are indicated in the legend.
- **Figure S4.** (a) The fraction of absorption and PL emission originating from *β*-conformation chains within 100 nm PODPF thin films, estimated by Gaussian peak fitting and spectral subtraction methods, as a function of annealing temperature. Sigmoidal curves are displayed to guide the eye. (b) The fraction of *β*-conformation PL emission as a function of the fraction of *β*-conformation chains. The corresponding data for *β*-conformation PFO films is also displayed for comparison.
- **Figure S5**. Time resolved spectra for varying time delay bins (left) for PODPF *β*-conformation self-doped thin films in the time range out to 1ns. (Right) A comparison of the extreme cases of disordered non-planar PL at early times and *β*-conformation PL at later times, together with a time integrated spectrum.
- **Figure S6**. Area normalised (left) and un-normalised (right) time resolved spectra for varying time bins for a PODPF *β*-conformation self-doped film over a 4 ns total time window.
- **Figure S7**. Time resolved spectra for varying time bins (left) for a PODPF disordered film. (Right) A comparison of the extreme cases of disordered non-planar PL at early times and *β*-conformation PL at later times, together with a time integrated spectrum.
- **Figure S8.** ASE peak FWHM and output intensity as a function of excitation pump energy for PODPF disordered (left, 461 nm) and *β*-conformation (right, 483 nm) chains.

Film preparation and characterization. Thin films of PODPF were spin coated at 2000 rpm for 60s from 10 mg/mL Chloroform solution onto fused silica substrates (12x12 mm, Spectrosil 2000, UGQ optics) at room temperature, giving 100 ± 10 nm films (thickness was measured using a Bruker Dektak XT stylus profiler). Films were annealed within an oxygen-free N_2 environment on a Linkam heating stage, controlled by a Linkam TP-93 controller. The stage was calibrated with a Testo surface thermometer with ± 1 °C accuracy to ensure accurate annealing temperatures. Each film was annealed on the pre-heated stage at a series of temperatures for 3 minutes each, with temperatures increasing step-wise, e.g. sequentially at 210, 225, 240, 255 °C. After annealing, films were removed from the heating stage and quickly transferred in air to a metal plate and allowed to cool to room temperature. The annealing temperatures used varied between 190 and 300 °C. After annealing at each temperature, the transmission and PL of the films was measured to characterise the temperature dependence of the β-conformation chain formation. Atomic force microscope (AFM) images were obtained using a Dimension 3100 (Veeco, CA) instrument in tapping model with a Si tip (resonance frequency: 320 kHz; spring constant: 42 N/m).

Optical analysis. Absorbance spectra were measured with a Shimadzu UV-3600 spectrometer and photoluminescence (PL) emission spectra were recorded on a Shimadzu RF-5301(PC) luminescence spectrometer, at 25 °C. Additional transmission measurements were performed with a Shimadzu UV-2550 spectrophotometer, with a slit width of 1 nm to ensure fine resolution of the β-phase vibronic absorption features. All films exhibited Fabry-Perot oscillations in the transmission at longer (non-absorbing) wavelengths > 460 nm and low losses due to scattering, demonstrating high-quality interfaces between substrate and film and good film uniformity. PL measurements were performed using a HORIBA Scientific FluoroMax-4 spectrophotometer, selectively exciting the disordered phase absorption peak at 385 nm.

Time-resolved PL measurements were performed with a Streakscope, simultaneously collecting emitted photons as a function of delay time from the pump pulse, Δt, and emission energy. The samples were excited with a laser at λ_{exc} = 379 nm. The FWHM of the pump pulse was ~60 ps, and the spectral resolution of the detector was 0.1 nm.

Low temperature measurements were performed within a cryostat, in a Helium gas environment. The samples were excited at λ_{exc} = 405 nm with a Fianium supercontinuum laser, and emission collected with an optical fibre interfaced via a spectrometer to an Andor charge coupled device (CCD) array. The PL intensity was calibrated using an Ocean optics HL-200-cal calibration light source with a known spectral response.

ASE Characterization: For gain measurements, planar waveguides were formed by spin-coating PODPF self-doped films onto polished synthetic quartz substrates. The samples were optically pumped with a Q-switched, neodymium ion doped yttrium aluminum garnate [Nd^{3+}:YAG] laser-pumped optical parametric oscillator (OPO) that delivered 10 ns pulses at a 10 Hz repetition rate. The pump wavelength was chosen to match the absorption maximum of the polymers. The pulse energy incident on the sample was adjusted by insertion of calibrated neutral density filters into the beam path. The pump beam was focused with a cylindrical lens and spatially filtered through an adjustable slit to create a 400 μm × 4 mm excitation stripe on the sample. At sufficient excitation intensity, the spontaneously emitted photons that are wave guided along the stripe-shaped gain region are amplified via stimulated emission.

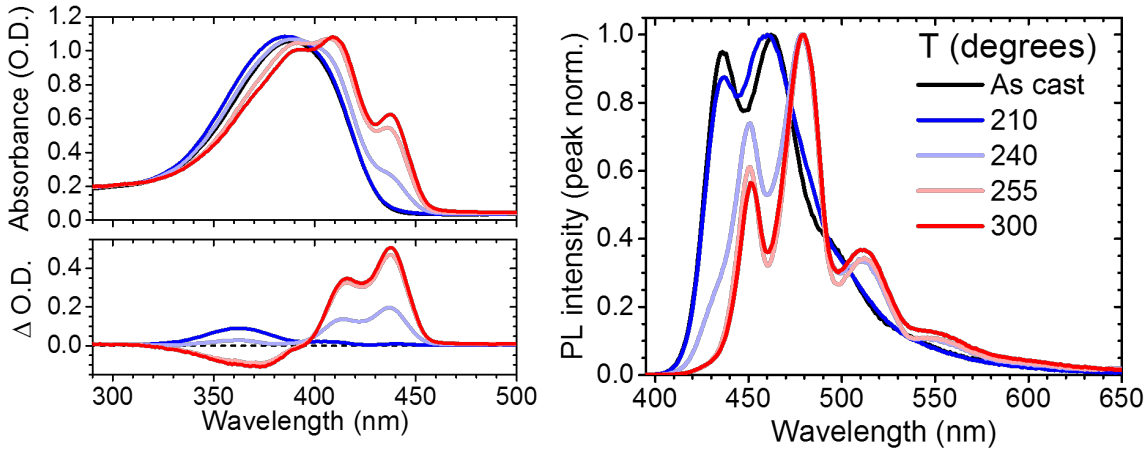

Figure S1. (Left) Absorbance spectra for a 100 nm PODPF thin film before and after annealing sequentially for 3 minutes at increasing temperatures. The lower panel shows the change in absorbance after annealing compared to the as cast film. (Right) The corresponding peak normalised PL spectra for the sequentially annealed PODPF film.

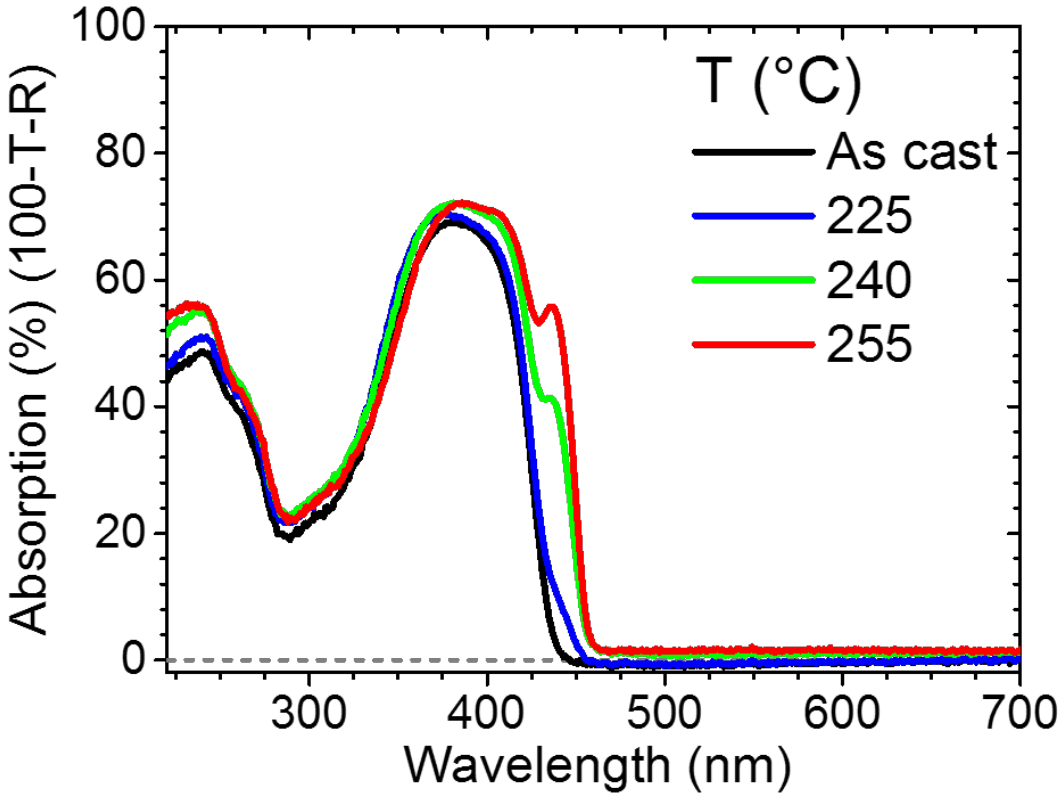

Figure S2. Reflection corrected absorption spectra for 100 nm thickness PODPF films after step-wise annealing at 210, 225, 240 and 255°C.

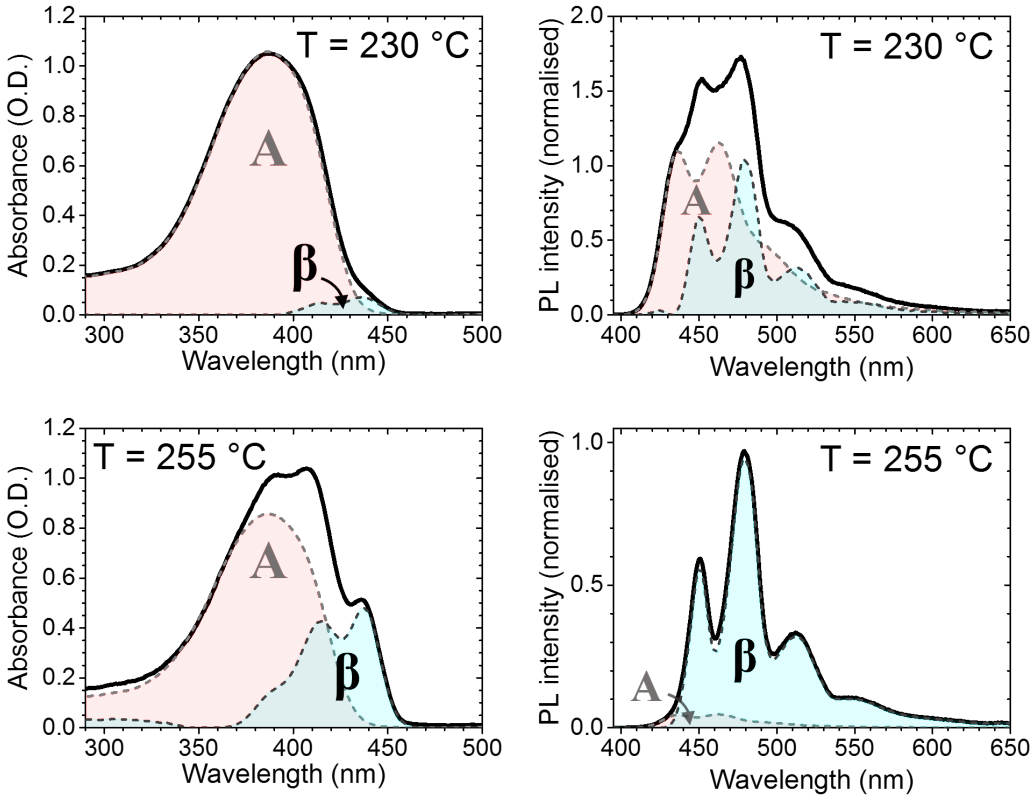

Figure S3. Example PODPF absorbance and PL spectra (for 230 and 255°C annealed samples) separated into their disordered (A) and *β*-conformation components using Gaussian peak fitting and normalisation and subtraction methods.

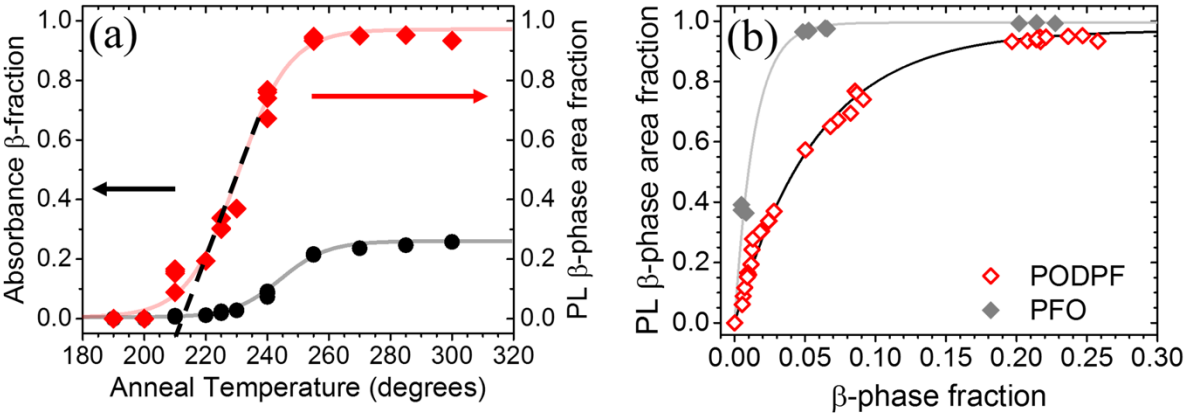

Figure S4. (a) The *β*-conformation absorbance (left ordinate, black data points) and PL (right ordinate, red data points) fractions as a function of annealing temperature for 100 nm thickness PODPF films, estimated by Gaussian peak fitting and spectral subtraction methods. Sigmoidal curves are shown as a guide to the eye. The dashed line tangent suggests a critical onset temperature of ≈ 210°C. (b) The fraction of *β*-conformation PL emission as a function of the fraction of *β*-conformation chains (estimated from the absorbance data). The corresponding data for PFO films is also displayed for comparison. Fitted inverse exponential functions for both data sets are displayed by the solid lines.

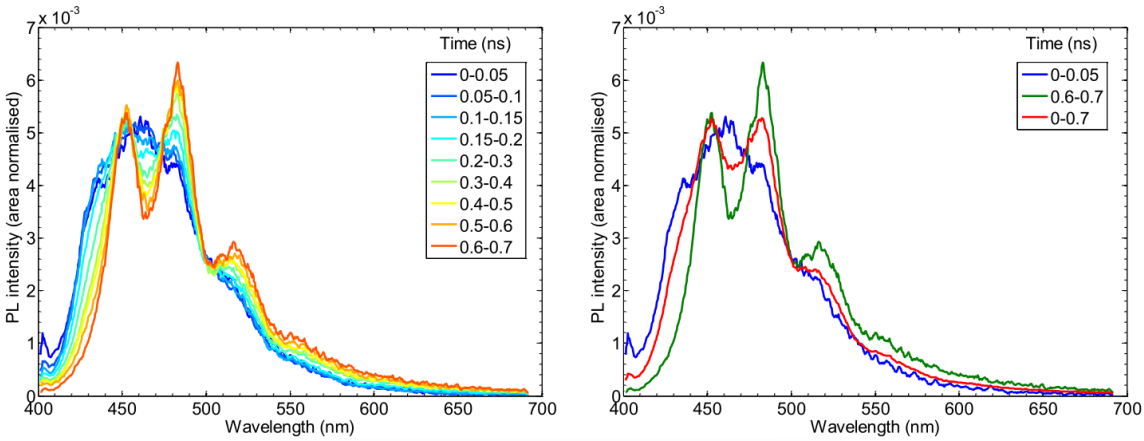

Figure S5. (Left) Time resolved PL spectra collected in different streakscope time bins for a PODPF β-conformation self-doped thin film across a time range from 0 to 1ns. (Right) Comparison of the extreme cases where disordered chain PL emission (blue line) dominates at early times and β-conformation emission (green line) at later times. The PL time-integrated across the whole range is also shown (red line).

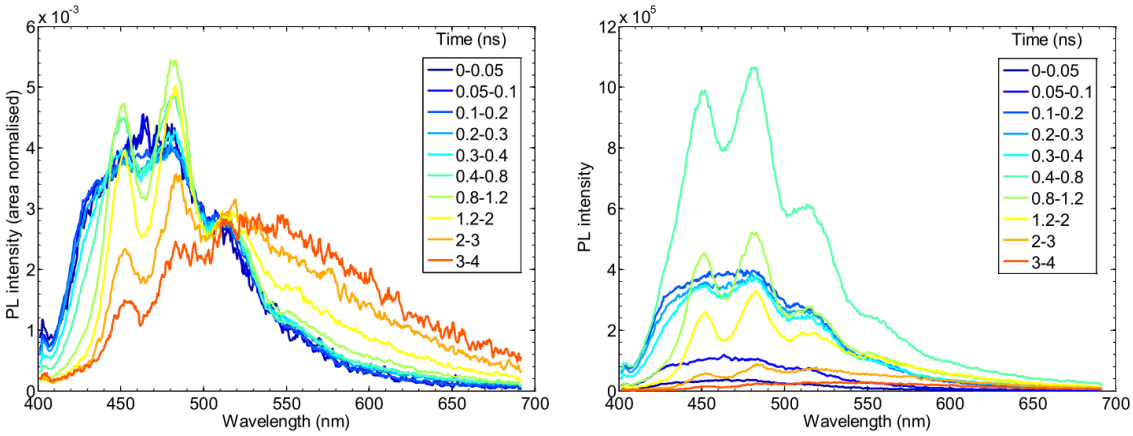

Figure S6. (Left) Area normalised and (Right) un-normalised time-resolved PL spectra collected in different Streakscope time bins for a PODPF β-conformation self-doped thin film across a longer time range from 0 to 4ns.

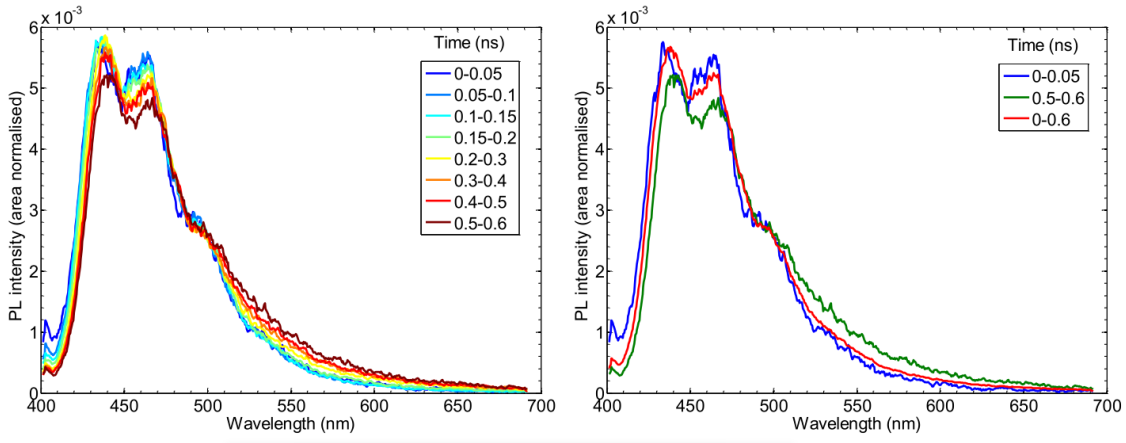

Figure S7. (Left) Time resolved PL spectra for different Streakscope time bins for a disordered PODPF thin film. (Right) Comparison of the PL emission observed at the earliest (blue line) and latest (green line) times, together with the PL time-integrated across the whole range (red line).

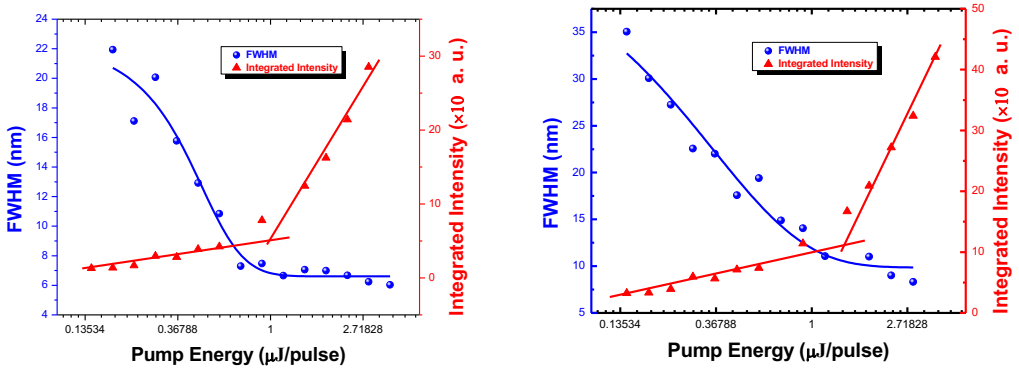

Figure S8. ASE full-width at half-maximum (FWHM) and output intensity as a function of pump energy for (Left) disordered PODPF (461 nm peak) and (Right) *β*-conformation PODPF (483 nm peak) films.